Tectonophysics 630 (2014) 137–149

Contents lists available at ScienceDirect

Tectonophysics

journal homepage: www.elsevier.com/locate/tecto

Foreland segmentation along an active convergent margin: New constraints in southeastern Sicily (Italy) from seismic and geodetic observations

Carla Musumeci [a], Luciano Scarfì [a,*], Mimmo Palano [a], Domenico Patanè [a,b]

[a] Istituto Nazionale di Geofisica e Vulcanologia, Sezione di Catania – Osservatorio Etneo, P.zza Roma, 2, Catania, Italy
[b] Instituto Andaluz de Geofísica, Campus Universitario de Cartuja s/n, Universidad de Granada, 18071 Granada, Spain

ARTICLE INFO

Article history:
Received 11 December 2013
Received in revised form 17 March 2014
Accepted 12 May 2014
Available online 20 May 2014

Keywords:
Southeastern Sicily
Seismotectonics
Tomography
Focal mechanisms
Crustal stress
Geodetic strain rate

ABSTRACT

We performed an in-depth analysis of the ongoing tectonics of a large sector of southern Sicily, including the Hyblean Foreland and the front of the Maghrebian Chain, as well as the Ionian Sea offshore, through the integration of seismic and GPS observations collected in the nearly two decades. In particular, a dataset consisting of more than 1100 small-to moderate-magnitude earthquakes ($1.0 \leq M_L \leq 4.6$) has been used for local earthquake tomography in order to trace the characteristics of the faulting systems, and for focal mechanisms computation to resolve the current local stress field and to characterise the faulting regime of the investigated area. In addition, GPS measurements, carried out on both episodic and continuous stations, allowed us to infer the main features of the current crustal deformation pattern. Main results evidence that the Hyblean Plateau is subject to a general strike–slip faulting regime, with a maximum horizontal stress axis NW–SE to NNW–SSE oriented, in agreement with the Eurasia–Nubia direction of convergence. The Plateau is separated into two different tectonic crustal blocks by the left-lateral strike–slip Scicli–Ragusa Fault System. The western block moves in agreement with central Sicily while the eastern one accommodates part of the contraction arising from the main Eurasia–Nubia convergence. Furthermore, we provided evidences leading to consider the Hyblean–Maltese Escarpment Fault System as an active boundary characterised by a left-lateral strike–slip motion, separating the eastern block of the Plateau from the Ionian basin. All these evidences lend credit to a crustal segmentation of the southeastern Sicily.

1. Introduction

Foreland segmentation, approaching an active convergent margin, has been widely observed worldwide. Among others, active segmentation was recognised along the Kuqa foreland basin of the Tarim Basin (Lu et al., 2000) and the Junggar Basin in China (He et al., 2004), along the Qilian Shan at the margin of NE Tibet (Tapponnier et al., 1990), at the Sierras Pampeanas, at the eastern margin of Central Andes (Iaffa et al., 2013), and along the eastern margin of Italy in the Adriatic–Apulian foreland (Oldow et al., 2002). The mechanism of segmentation depends on several factors such as the convergence rate variations along the convergent margin strike, the basement structures, the block thickness, the rock strength, etc. (e.g. Jordan et al., 2001). Furthermore, the patterns may be complicated by the presence of pre-existing structures that can be reactivated in order to accommodate the deformation related to the convergence process. Here we focus on the Hyblean Foreland (or Hyblean Plateau in Fig. 1a), one of the most seismically hazardous zones in the central Mediterranean region, where the presence of active faults suggests a possible segmentation of it.

The current tectonic setting of the Hyblean Foreland is related to the long-term Eurasia and Nubia convergence (e.g. Faccenna et al., 2001; Fig. 1). The boundary of these plates, running through Sicily and the Ionian Sea, gives rise to a very complex tectonic framework, with several tectonic blocks, in which all of the structural domains characterising a collisional belt are exposed: the Maghrebian fold-and-thrust Belt, the Gela-Catania Foredeep, the Pelagian Block and, further to the east, the subduction complex of the Ionian oceanic basin beneath the Calabro-Peloritan Arc (see Finetti et al., 2005; Mantovani et al., 2009 and references therein). The outcome of this structural framework is the high seismic potential that characterises the region. In particular, in historical times it experienced several destructive events such as the 1169 and 1693 earthquakes (MCS intensities of XI, with estimated magnitudes of about 7 or higher; Boschi et al., 2000), and more recently, a $M_L = 5.4$ earthquake occurred on December 13, 1990, about 10 km offshore (Amato et al., 1995).

Recent advances achieved through geological (e.g. Barreca, 2014; Bousquet and Lanzafame, 2004; Catalano et al., 2008), petrological (Manuella et al., 2013), seismological (Brancato et al., 2009; Musumeci et al., 2005; Presti et al., 2013; Scarfì et al., 2007) and geodetic studies (e.g. Devoti et al., 2011; Ferranti et al., 2008; Mattia et al., 2012; Palano et al., 2012) have contributed to depict the rough picture of the

* Corresponding author.
E-mail address: luciano.scarfi@ct.ingv.it (L. Scarfì).

http://dx.doi.org/10.1016/j.tecto.2014.05.017
0040-1951/

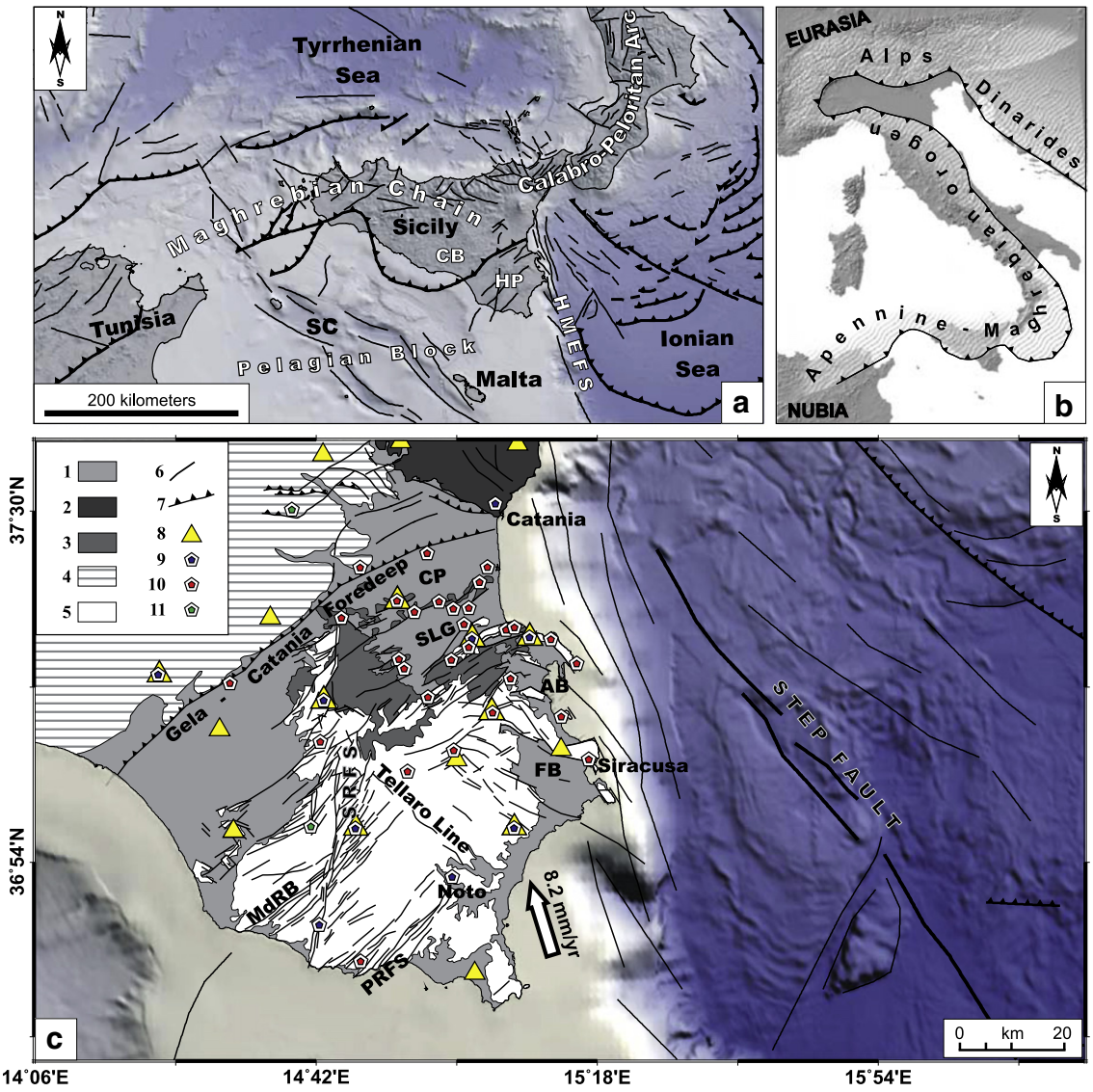

Fig. 1. Simplified tectonic map of Sicily (a); abbreviations are: SC, Sicily Channel; HP, Hyblean Plateau; CB, Caltanissetta Basin; HMEFS, Hyblean–Maltese Escarpment Fault System. The Maghrebian Chain and the Calabro Peloritan Arc are parts of the Apennine–Maghrebian orogen (b), a large scale fold-and-thrust belt formed during the Neogene-Quaternary convergence between Nubia and Eurasia plates. (c) Simplified structural sketch map of southeastern Sicily: 1) Recent-Quaternary sedimentary deposits; 2) Late Pleistocene-Holocene Etnean volcanics; 3) Plio-Pleistocenic Hyblean volcanics; 4) Maghrebian Chain units; 5) Meso-Cenozoic carbonate sediments; 6) main faults, 7) main thrust fronts; 8) seismic stations; 9) continuous GPS stations; 10) episodic GPS benchmarks; 11) GPS solutions coming from Ferranti et al. (2008). Abbreviations are: CP, Catania Plain; SLG, Scordia–Lentini Graben; AB, Augusta Basin; FB, Floridia Basin; PRFS, Pozzallo-Rosolini Fault System; MdRB, Marina di Ragusa Basin; SRFS, Scicli–Ragusa Fault System. Tectonic structures redrawn from Catalano et al. (2010) and Polonia et al. (2011). The white arrow shows the convergence vectors between Nubia and Eurasia according to the Morvel Plate model (DeMets et al., 2010).

tectonic features in southeastern Sicily. However, several aspects related to the ongoing tectonic processes and to the geometry, kinematics and dynamics of individual faults or fault arrays have still not been satisfactorily explored. Moreover, there is a poor consensus regarding the location and extent of the faults involved in the historical earthquakes. As an example, various causative sources (Visini et al., 2009) have been suggested for the 1693 earthquake (Fig. 2), which struck a large portion of eastern Sicily, affecting with maximum intensities the area around Catania and the whole Hyblean Plateau (Guidoboni et al., 2007). These sources range from the Hyblean–Maltese Escarpment Fault System (e.g. Argnani and Bonazzi, 2005; Azzaro and Barbano, 2000; Bianca et al., 1999) to a NNE-oriented 60 km long-fault nearly overlapping the Scicli–Ragusa Fault System (Sirovich and Pettenati, 2001) or to a segment of the S-verging basal thrust of the Maghrebian Chain (Lavecchia et al., 2007). Consequently, the detection and the characterisation of active and seismogenic crustal faults, as well as an improved image on the active tectonic processes, ensure a significant challenge in this area.

Exploiting local monitoring network high-quality data, we performed an in-depth analysis of the ongoing tectonics of southeastern Sicily, through the integration of seismic and GPS-based geodetic observations collected in nearly two decades. In particular, we carried out a simultaneous inversion of both 3D velocity structure and distribution of seismic foci. This resulted in more accurate hypocentres and into mapping the velocity anomalies, which, being strictly dependent on the crustal structure, is of help in the seismotectonic interpretation by tracing the characteristics of a faulting system. In addition, the fault plane solutions for the best recorded earthquakes were determined and used to resolve the current local stress field and to characterise the faulting regime of the main seismogenic sources. Moreover, a dense combination of continuous and episodic GPS measurements allowed us to infer the main features of the current crustal deformation pattern. The results were combined to

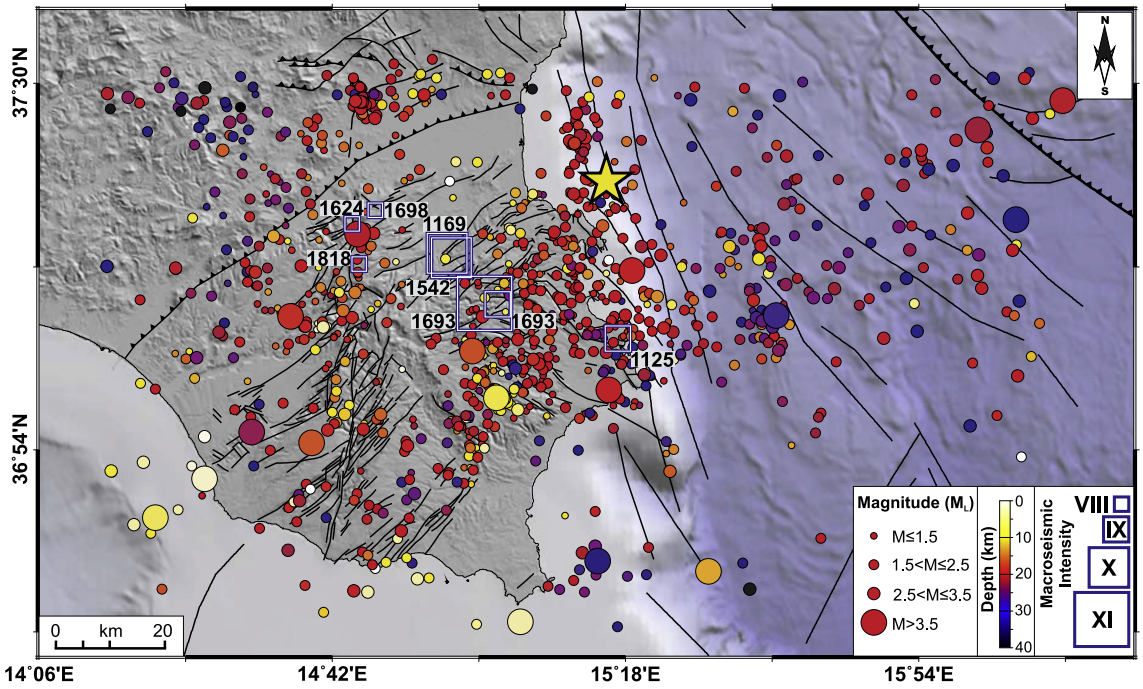

Fig. 2. Routine earthquake locations from 1994 to 2013 and historical earthquakes are shown by circles and squares, respectively. Star shows the location of the M_L 5.4 1990 earthquake (from Amato et al., 1995). Historical earthquakes are from Guidoboni et al. (2007). See inset for symbols and colours.

achieve a coherent geodynamic scheme and to better characterise the active tectonics of the region.

2. Tectonic setting

The current geological–structural setting of southeastern Sicily must be considered in the frame of the complex tectonic features of the Mediterranean basin, which is dominated by the ~N20°W (according to the Morvel plate model; DeMets et al., 2010) Neogene-Quaternary convergence between Nubia (the African plate west of the East African Rift) and Eurasia plates (Faccenna et al., 2001).

Southeastern Sicily is mostly represented by the Hyblean Foreland (HP in Fig. 1a), consisting of an isolated and elevated forebulge structure formed since the early Miocene time by bending of the foreland lithosphere beneath the load of the advancing Maghrebian Chain (Billi et al., 2006). It is located at the northeastern end of the mostly submerged Pelagian Block extending up to Sicily Channel, the Maltese islands and Tunisia (e.g. Boccaletti et al., 1990; Malinverno and Ryan, 1986; Patacca et al., 1990). The autochthonous sedimentary wedge (about 7 km thick) consists of Triassic to Pleistocene carbonate succession with intercalated dominantly submarine hydro- and volcaniclastic units and minor lava flows (Grasso et al., 2004). At the present, the Plateau plays the role of a crustal indenter that, confined between the flexured continental crust area of the Caltanissetta Basin (Fig. 1a), to the west, and the oceanic domains of the Ionian Basin Sea (Finetti and Del Ben, 1996), to the east, has impinged against the front of the Maghrebian Chain.

Eastward, the Hyblean Foreland is bounded by the NNW–SSE-striking Hyblean–Maltese Escarpment Fault System (HMEFS in Fig. 1a), a Mesozoic lithospheric boundary separating the Pelagian Block continental crust from the Ionian oceanic basin (Nicolich et al., 2000; Torelli et al., 1998). The HMEFS has been interpreted as a right lateral active transtensional system overprinting the pre-existing Mesozoic continent–ocean transition between Sicily and the Ionian basin (Doglioni et al., 2001). Recently, Argnani and Bonazzi (2005) suggested that along the segment north of Siracusa, the Hyblean–Maltese Escarpment is characterised by active faults while the southern part is not affected by lithospheric tearing. Seismic reflection profiles and bathymetric surveys also revealed the existence, eastward of HMEFS, of active faults segmenting the Ionian subduction complex (Fig. 1c). Among these, a structure, located about 70 km eastward of the coastal line, has been interpreted either as a crustal-scale structure marking the continent–ocean boundary of the Ionian oceanic basin (Chamot-Rooke et al., 2005) or as a major lithospheric structure that accommodates different rates of slab motion (STEP fault in Fig. 1c; Polonia et al., 2011).

On the other hand, the northern and the northwestern margins of the Hyblean Plateau are flexed and downbent to form a foredeep basin floor beneath the Catania Plain (Fig. 1c). The collapse of the foreland plate margin was coupled with progressive forelandward migration of the Maghrebian thrust wedge (the Gela-Catania Foredeep) into precursor late Neogene and the successor Pleistocene foredeep basins (Butler et al., 1992). The frontal thrust belt was considered locked since the Middle Pleistocene (Butler et al., 1992; Tortorici et al., 2001), but recent studies, based on geological (Bousquet and Lanzafame, 2004; Catalano et al., 2008; Spampinato et al., 2013), seismological (Lavecchia et al., 2007; Visini et al., 2010) and geodetic (see Palano et al., 2012 for an overview) observations have detected the occurrence of active contraction.

Westwards, the Hyblean Plateau is cut by a major N–S oriented shear zone, 70 km long, known as Scicli line or Scicli–Ragusa Fault System (SRFS in Fig. 1c; Ghisetti and Vezzani, 1980; Grasso and Reuther, 1988). Extending from the frontal thrust belt of the Appennine–Maghrebian Chain (in the north) to the southern offshore, it is formed by three NS-trending main fault segments and second-order structures with NE–SW en-echelon arrangement that accommodate the shear deformation (Catalano et al., 2010). Available seismic reflection lines allow the Scicli offshore to be mapped for a minimum length of 40 km (Grasso et al., 2000). The geometry of the SRFS, as a whole, is the product of a prolonged dextral strike–slip deformation that reactivated a Cretaceous-Late

Tertiary fault zone (Grasso and Reuther, 1988). The effects of the dextral motions are well evidenced by the development of both restraining and releasing bends between the distinct en-echelon segments of the fault system. However, detailed geological studies (e.g. Catalano et al., 2008) have inferred that since about 0.85 Myr, the northern fault segments of the SRFS, have been partially reactivated by left-lateral motions.

Furthermore, recent morphological features of the Hyblean Plateau result from the extensional tectonics that affected this region during the Quaternary (e.g. Bianca et al., 1999). In the northeastern and southwestern borders of the plateau, two N50°E-oriented tectonic troughs, the Scordia–Lentini Graben and the Marina di Ragusa Basin (SLG and MdRB in Fig. 1c), can be recognised. In the eastern part, the NW–SE oriented basins of Augusta–Siracusa and Floridia (AB and FB in Fig. 1c) correspond to tectonic depressions separated by uplifted ridges controlled by impressive normal fault segments.

3. Seismic data

In total 1128 small-to moderate-magnitude earthquakes ($1.0 \leq M_L \leq 4.6$) have been recorded in southeastern Sicily between January 1994 and March 2013 by a local network operated by the Istituto Nazionale di Geofisica e Vulcanologia (yellow triangles in Fig. 1c). This network configuration, originally equipped with three component short-period sensors (Musumeci et al., 2005), has been considerably enhanced since 2005 by 24 bit digital stations equipped with broadband sensors. The events (Fig. 2), selected from the "Catalogo dei terremoti della Sicilia Orientale - Calabria Meridionale, INGV, Catania" (Gruppo Analisi Dati Sismici, 2013), have been employed as data source for a simultaneous inversion of a 3-D velocity structure and hypocentre parameters and focal mechanism computations (see also Scarfì et al., 2013 for a focal mechanism comparison).

3.1. Crustal structure and earthquake location

The seismic velocity modelling of southeastern Sicily was carried out by applying the tomoDDPS algorithm (Zhang et al., 2009), which is able to solve simultaneously for V_P, V_S and V_P/V_S ratio. Compared to more simple algorithms, this code uses a combination of both absolute and differential arrival time readings, between couple of events of an earthquake cluster. This essential feature allows to considerably improve the relative locations and to sharpen the velocity images near the source region, preventing also the risk that velocity perturbations outside the well illuminated area are mapped into it. Moreover, including of the S–P times, the code produces a reliable V_P/V_S model, avoiding to get it by means of a simple division of P and S models, which could be different in quality and resolution.

For the tomographic inversion, the initial dataset was filtered according to the quality criteria of location. In particular, we selected only events with at least seven observations (P- and S-phases), root-mean-square (RMS) residuals smaller than 0.35 s and horizontal and vertical location errors lower than 3.5 km and 4.5 km, respectively. The final dataset consists of about 880 earthquakes (see Fig. A1 in the Auxiliary Materials) with a total of 6131 P and 3668 S absolute arrival times and 52980 P and 30138 S catalogue-derived differential times. Following the one-dimensional reference velocity model of Musumeci et al. (2003), data inversion has been performed by considering an horizontal grid of 7 × 7 km node spacing (covering an area of 110 × 110 km) and a vertical step varying between 3 and 6 km, from the surface to 28 km of depth. This mesh configuration allowed to achieve a better spatial resolution with respect the other tomographic studies carried out in the region (Brancato et al., 2009; Scarfì et al., 2007), also ensuring a good over-determination factor (i.e. the ratio between known and unknown parameters).

As first hint to assess the calculated model quality, we considered the zones with a reasonable illumination, plotting the derivative weigh sum (DWS), a statistical parameter which quantifies the ray density around each model node. Overall, travel time residuals, DWS and other parameters furnish first-order diagnostics for the assessment of the resolution, whose real significance depends on the individual conditions of the inversion problem and whose understanding needs intuition.

Hence, we carried out numerical experiments with synthetic models, which give an immediate and straightforward idea of the inversion stability, potentially insignificant or artificial features and the sensitivity with respect to the choice of the starting model. In practice, we calculated theoretical travel times for some velocity test models (i.e. chequerboard and characteristic models; for details about the test procedures see Husen et al., 1999 and Scarfì et al., 2007, 2009). The synthetic data were inverted using the same starting model and control values as for the real data. Then, we checked the zones where the target models (i.e. test models) were not restored (low resolution areas). As expected, these tests proved that large sectors of the investigated volume, coinciding with areas with a reasonable illumination (DWS $\geq$ 100 for V_P and $\geq$50 for V_S), fulfil the requirements for the interpretation (see Fig. A2 in the Auxiliary Materials).

Maps and sections in Figs. 3 and 4 display the 3D V_P velocity model obtained. The tomographic images reveal several sharp lateral velocity perturbations pointing out meaningful discontinuities in the crust, which can be related to the major tectonic structures. In particular, in the north-western sector, about corresponding with the Gela-Catania Foredeep, a clear low V_P anomaly, striking about NE–SW (NW dipping), is recognisable between 3 and 20 km of depth. Location and geometry of this feature suggest that it may be related with the Hyblean crust bending beneath the Maghrebian Chain. Coastal and offshore zones, from Catania to Siracusa, are accompanied by considerable velocity contrasts, well identifiable down to a depth of about 20 km. These anomalies likely mark the known fault systems, striking about NNW–SSE to N–S, such as the HMEFS and those faults bounding the Augusta Basin. Toward south, a deep low velocity zone, trending NE–SW, characterises a band near the coast. Finally, in the western sector, velocity anomalies between 36.9 and 37.3 of latitude well mark at depth the existence of the Scicli–Ragusa Fault System, highlighting discontinuities striking about N–S and NE–SW.

S-wave velocity structure, retrieved by the inversion, exhibits a very similar trend to that of the V_P, while the images of the V_P/V_S (Figs. 3 and 4) show widespread high values (1.8–1.9) overlapping seismic layers and neighbouring zones, which might be indicative of highly fractured zones (e.g. O'Connel and Budiansky, 1974; Thurber et al., 1997).

Current results, compared to the previous tomographic inversion of Scarfì et al. (2007), maintain the fundamental characteristics but at the same time show an improved detail, thanks to the larger amount of available data, which results in a higher density of seismic rays sampling the spatial mesh.

The finely tuned velocity distribution was then used to relocate by TomoDDPS code the whole dataset of events recorded in the investigated region. This provided an improvement in the quality of the final locations, reducing the average travel time residual (RMS) of about 70%, with almost all of events having a final RMS smaller than 0.1 s, and an higher clustering which emphasizes lineaments, some of which corresponding to the crustal discontinuities pinpointed by the velocity images. However, the seismicity is neither uniformly distributed nor confined to one linear zone (Fig. 5). To the north and northwest, earthquakes appear distributed along the edge between the foreland and the chain, with depth increasing toward NW, down to about 40 km, to outline a flexure of the seismogenic layer below the chain domain. Toward south, in the western district, the epicentres finely overlap to the Scicli–Ragusa Fault System, along the main direction striking about N–S and the NE–SW associated structures. Moving eastward, seismic events are concentrated in the area between Siracusa, Noto, Palazzolo Acreide and Augusta, where the typical seismogenic depth is between 15 and 25 km. Seismicity becomes sparse or lacking beyond the onshore edges of this zone of the plateau, namely to the south, to the north (in the

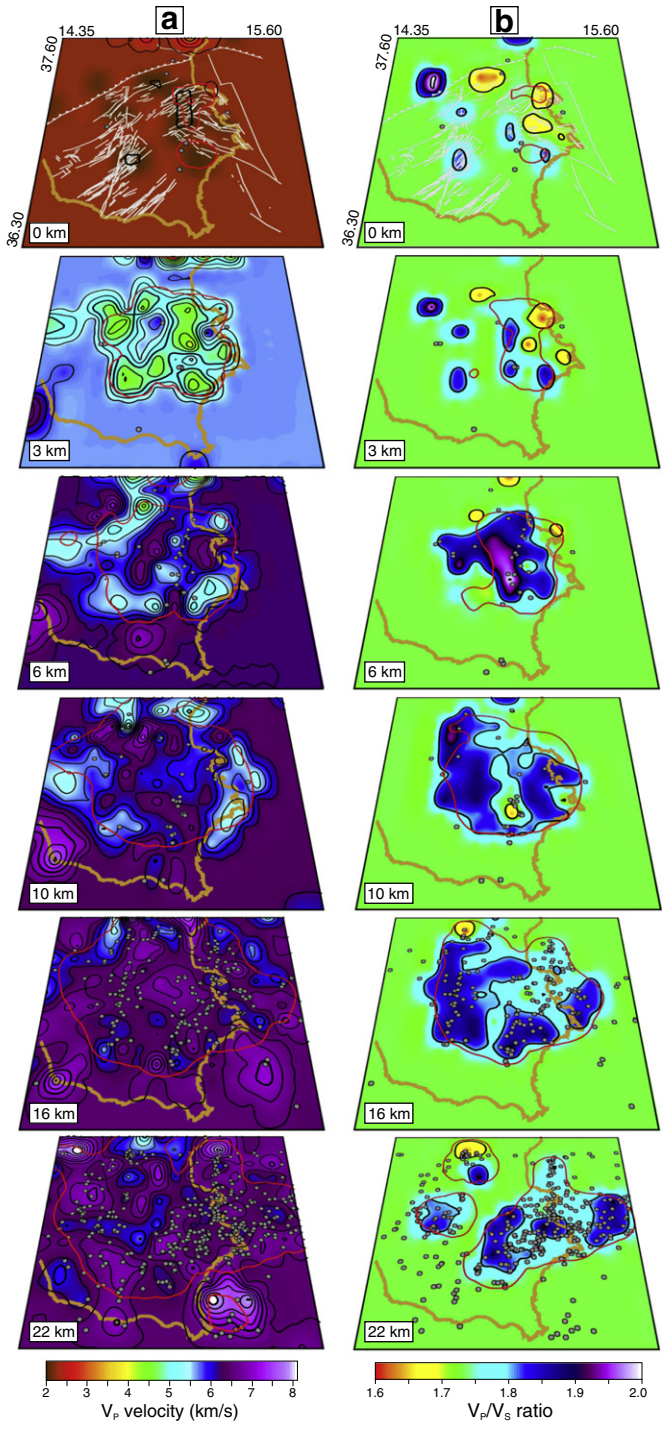

Fig. 3. V_P (a) and V_P/V_S (b) models for six representative layers resulting from the 3D inversion. Contour lines are at interval of 0.25 km/s for V_P and 0.1 for V_P/V_S. On the 0 km layer the main structural features are reported with white lines. Grey circles represent the relocated earthquakes within half the grid size of the slice. The zones with DWS > 100 (a) and DWS > 50 (b) are circumscribed by red contour lines.

Scordia–Lentini Graben area) and between the Scicli–Ragusa Fault System and the Tellaro Line (Fig. 5). Lots of the events are also concentrated along the coastal area, matching quite well the faults that border the Augusta and Floridia basins. In the plateau, the geometry of several clusters seems indicate the WNW–ESE direction as the main direction of the seismogenic structures. In the nearby Ionian offshore, earthquakes lie along the HMEFS, between Catania Gulf and Siracusa, while a cluster, striking in NNW–SSE direction, is detectable 30 km east from Siracusa. Further east, events are scattered, although some NW–SE lineaments can be traced. Here the seismogenic depths range between 20 and 40 km, but this last finding must be read with caution as the geometrical gap of the network could create artefacts.

3.2. Focal mechanisms and stress inversion

In this study, we used FPFIT algorithm (Reasenberg and Oppenheimer, 1985) for focal mechanism determination. It is a simple and conventional method using P-wave polarity data and their spatial distribution on the focal sphere. First, polarities were accurately re-picked from the digital seismic waveforms, then the algorithm, with rays traced through the computed 3D velocity model, has been used.

From the initial dataset of 195 earthquakes with $M_L > 1.2$ and at least 8 clear P-wave polarities (71% of the 195 shocks had 10 or more first-motion readings, 15 on average), we discarded fault-plane solutions (FPSs) with any one of the following criteria: i) ratio NDisc/NPol (NDisc is the number of discrepant observations and NPol is the number of first readings used in the solution) greater than 0.2; ii) large uncertainty in P- and T-axis orientation and regions overlapped; iii) averaged uncertainties in strike, dip and rake greater than 20°, and iv) number of multiple solutions greater than 2. The selection criteria yielded 165 well-constrained FPSs. Locations and corresponding fault plane solutions are given in Fig. 6, while focal parameters of each event are given in Table S1 of the Auxiliary Materials.

All types of mechanisms are represented, although strike–slip solutions outweigh normal and reverse ones (Fig. 6). In particular, most of the solutions exhibit left-lateral strike–slip motions on fault planes that strike NE–SW up to N–S or dextral–lateral strike–slip motions when the NW–SE striking planes are considered (Fig. 6). Only a small minority, namely seven events, exhibits reverse faulting, with rupture planes mainly northeast–southwest oriented. Nineteen events having normal faulting features on fault planes that strike mainly N–S (northwards) and NW–SE (southwards) are also observed. Thrust and normal faulting events are not concentrated in a special geographic zone or depth interval of the investigated area, but they seem to be spread randomly in space.

For each earthquake the projection of P- and T-directions, representative of the local maximum and minimum principal strain axis, is shown as inset in Fig. 6. The plot shows that the average compressive stress axis is nearly horizontal and in the NW–SE direction, while the tensional axes have an average trend that is nearly horizontal and in the NE–SW direction. Although some vertical compressive and tensional axes are observed, they are less numerous in comparison to the horizontal ones, confirming that they have much less quantitative importance than the strike–slip faulting.

Assuming that local faulting is controlled by large scale dynamics, the integrated analysis of seismic sources belonging to a given crustal block can supply information on the regional stress field (Wyss et al., 1992). To this purpose a standard numerical technique (Gephart, 1990; Gephart and Forsyth, 1984) has been applied to invert the 165 selected focal mechanisms and determine the principal stress axes (σ_1, σ_2, σ_3) and the dimensionless parameter $R = (\sigma_2 - \sigma_1) / (\sigma_3 - \sigma_1)$, which represents the shape of the stress ellipse. The method identifies the best stress tensor model that most closely matches all the fault plane solutions of the source region. It requires the basic assumption that the stress is uniform in space and time domains in the investigated volume. Moreover, a variable misfit (F), given by the angular difference between the observed slip direction on a fault plane and the shear stress derived from the stress model, is introduced in order to provide a guide to how well the assumption of stress homogeneity is fulfilled (Michael, 1987). Following Wyss et al. (1992), Gillard et al. (1996) and Cocina et al. (1997), we assumed that the condition of a homogeneous stress distribution is fulfilled if the misfit is smaller than 6° and that it is not fulfilled if F > 9°. For F values between 6° and 9° the solution is considered acceptable, but it may reflect some heterogeneities. We also computed

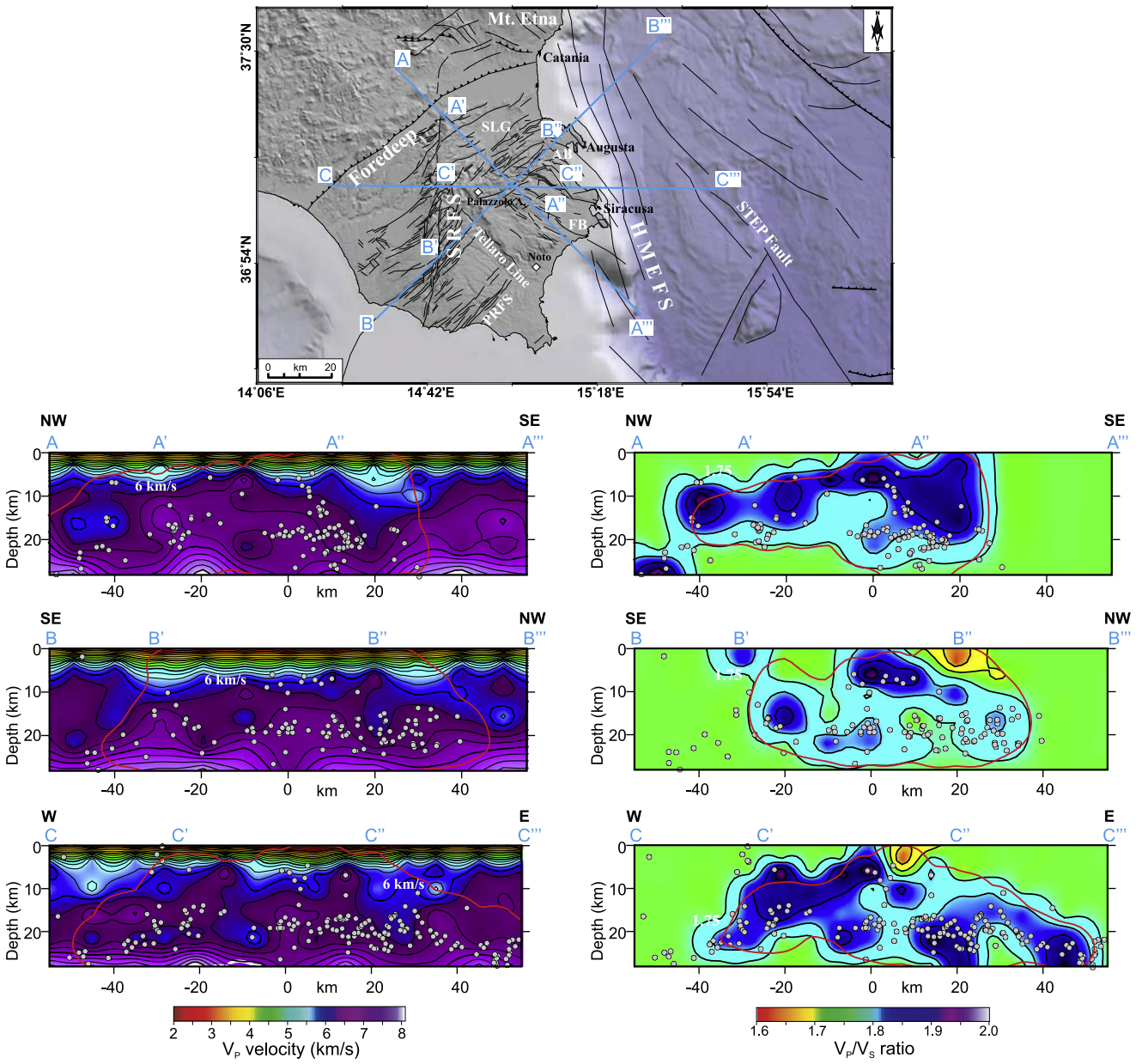

Fig. 4. Vertical sections through the V_P (left) and V_P/V_S (right) models. The traces of the sections (AA‴, BB‴ and CC‴) are reported in the sketch map. Contour lines are at an interval of 0.25 km/s for V_P and 0.1 for V_P/V_S. Red curves contour the zones with DWS > 100 for V_P and DWS > 50 for V_P/V_S. Relocated earthquakes, within ±10 km from the sections, are plotted as grey circles. Abbreviations as in Fig. 1.

the 95% confidence level, which states the degree to which a measure is constrained, using the statistical procedure described by Parker and McNutt (1980) and Gephart and Forsyth (1984).

The main findings for the entire dataset can be summarized as follows: F = 6.6°, R = 0.6, σ_1 = N320° dip 0°, σ_2 = N203°E dip 89°, σ_3 = N50°E dip 1° (dataset A in Table 1 and Fig. 7a). The results indicate that the area is affected by a strike–slip regime with a NW–SE compressive field, associated with a NE–SW tensional field. However, the average misfit of 6.6° indicates somewhat heterogeneous conditions.

Expecting that the subdivision of the dataset into smaller groups will give solutions with smaller misfits, we employed the cumulative misfit method (Wyss and Lu, 1995). The method is based on the cumulative misfit of individual fault-plane solutions, calculated assuming a reference stress tensor. Plotting the cumulative sum of misfits as a function of earthquake number (N), sorted by increasing depth, longitude or latitude, we may identify the points where the curve changes slope, indicating boundaries between regions of different stress. To reduce the subjectivity in the identification of changes in slope and to estimate the statistical significance of these changes, we computed the standard Z values resulting from the comparison of all possible divisions of the dataset in two halves (Wyss and Lu, 1995).

By using the overall average stress direction as a test tensor (dataset A in Table 1) and applying the Z test to the dataset ordered for growing depth or latitude, no break in slope has been identified. Conversely, two change in slope (significant at ≥95% confidence level), defining three areas of potentially different stress conditions, have been identified when growing longitude was considered (Fig. 7b). The first important change in slope occurs at earthquake number 38 (longitude of 14.753), the second change occurs at earthquake number 105 (longitude of 15.202). These longitude boundaries coincide roughly with the Scicli–Ragusa Fault System and the Hyblean–Maltese Escarpment Fault System (Fig. 1). Within each segment we performed separate inversions, all revealing stress tensors characterised by a strike–slip regime (datasets B, C and D in Fig. 7c and Table 1). The best-fit stress tensor for the events

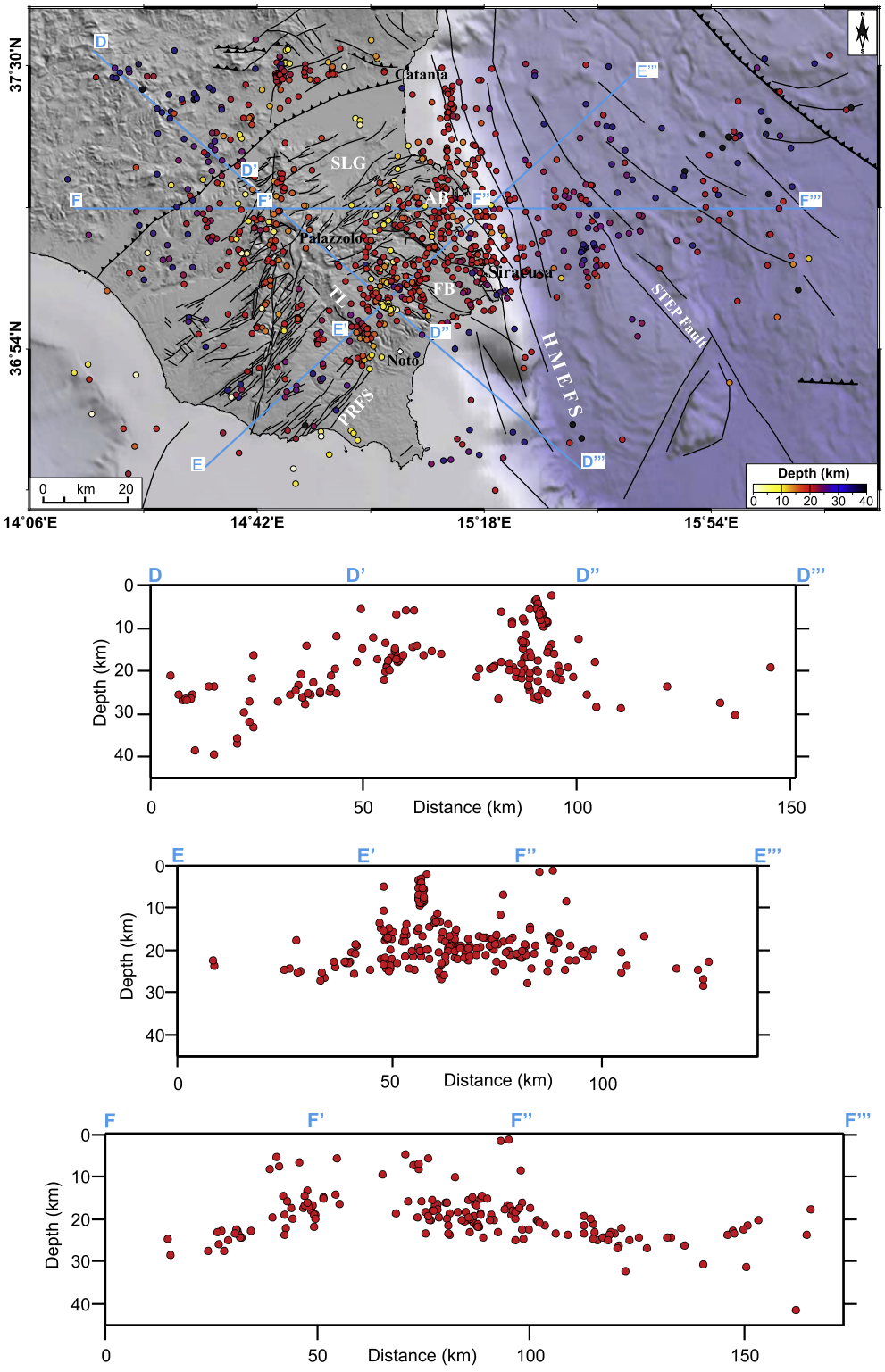

Fig. 5. Final event locations in map and vertical sections. The main fault systems and the traces of the sections (DD‴, EE‴ and FF‴) are also shown in map. TL, Tellaro Line; other abbreviations are as in Fig. 1.

to a longitude greater of 15.202 (datasets D) shows a low average misfit (F = 4.9) corresponding to a condition of homogeneous stress distribution. However, the attempt to reduce the average misfit in the Hyblean block to significantly lower values than F for the total dataset was futile (see datasets B and C in Table 1). Thus, we were left with the information that the stress tensor in the Hyblean block changes (from cumulative misfit), but we cannot reliably resolve how much it changes.

This is also confirmed (Fig. 8) by the inversions on a grid in map view obtained by using the software package ZMAP (Wiemer, 2001). All events inside a radius of 15 km around a grid cell 15 × 15 km spacing have been selected and their focal mechanisms inverted using Michael's approach (Michael, 1987). The resulting directions of the principal stress axes (σ_1) are plotted as lines on map along with the colour-code of the variance of the resulting inversion at each node. Blue to

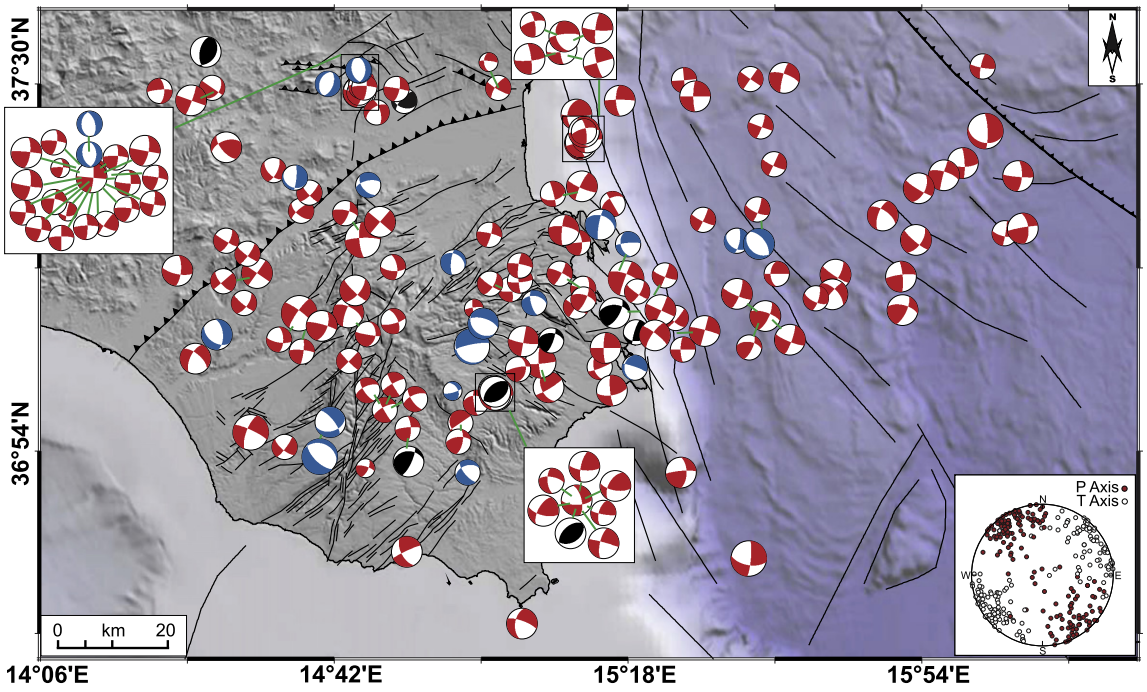

Fig. 6. Map of the 165 earthquakes selected for stress tensor inversion and relative focal plane solutions. Plunges of P- and T-axes have been used to divide focal mechanism datasets into the main stress regime categories, according to the Zoback (1992) classification: red, strike-slip fault; blue, normal fault; black, inverse fault. In the inset the projection of P and T directions.

red colours indicate an increase of variance. As obtained by the individual inversion results and their uncertainties using Gephart and Forsyth approach (1984), also in this case the Hyblean Plateau, showing red areas, highlights regions where only a poor fit to a homogeneous stress tensor has been obtained.

Summing up, the area, apart from local minor variations, is substantially undergoing a strike slip deformation with a difference in the extensional or compressional component in the blocks identified. In particular, the sector to the west shows a more relevant extensional component with respect to nearby blocks.

4. GPS data

Geodetic GPS-based monitoring of the Hyblean area is currently carried out since 2005 by INGV through the set-up of a permanent GPS network in the framework of the "Rete Integrata Nazionale GPS (http://ring.gm.ingv.it)". In addition, a network comprising a local trilateration network and a levelling route managed by the International Institute of Volcanology (merged into INGV in 2001) and the Istituto Geografico Militare Italiano (www.igmi.org) respectively, was surveyed in 1998, 2000, 2005 and 2006. In this study, in order to increase station density on the study area, we also analysed some measurements collected during the last decade mainly for mapping, engineering and cadastre purposes. All GPS data were processed by using the GAMIT/GLOBK software (Herring et al., 2010) following the strategy described in Palano et al. (2011). To improve the overall configuration of the network and tie the regional measurements to an external global reference frame, data coming from 12 continuously operating IGS stations (AJAC, BRUS, CAGL, GRAS, GRAZ, JOZE, LAMP, MATE, MEDI, NOTO, NOT1 and ZIMM; see Beutler et al., 2008 for details about the whole IGS stations) were introduced in the processing. To adequately show the crustal deformation pattern over the investigated area, estimated GPS velocities were aligned to a fixed Eurasian reference frame (Euler vector parameters: N55.963, E-97.169 and $\Omega = 0.262°$/My; Palano et al., 2013). The geodetic velocity map is reported in Fig. 9a.

Under the assumption that the crust deforms as a continuum medium (e.g. England and Molnar, 1997), we computed the 2D strain-rate tensor over the studied area. In particular, in a first step, by taking into account the observed horizontal geodetic velocity field and associated covariance information we derived a continuous velocity gradient tensor on a regular $0.1° \times 0.1°$ grid (whose nodes do not coincide with any of the GPS stations) using a "spline in tension" technique (Wessel and Bercovici, 1998). The tension is controlled by a factor T, where $T = 0$ leads to a minimum curvature (natural bicubic spline), while $T = 1$ leads to a maximum curvature, allowing for maxima and minima only at observation points (in our computations we set $T = 0.4$). Sites IGAT, IP18, IP03, IP13, PZLA, CLTG, POZZ, and CONS (reported as blue arrows in Fig. 9a) have not been used for the velocity gradient computation since they are biased by large uncertainties or show suspicious motion with respect to nearby sites. As a final step, we computed the average 2D strain-rate tensor as derivative of the velocities at the nodes of each grid cell. The estimated strain-rates are shown in Fig. 9b.

The geodetic velocity field depicts a general NNW-directed motion with an N–S increasing gradient across the Scordia–Lentini Graben, passing from values of about 3.0 mm/yr on the northern rim of the plateau itself to values of about 5.5 mm/yr, along the southern-central sector of the Hyblean Plateau (Fig. 9a). Sites installed across the northern sector of the Scicli–Ragusa Fault System show a diverging pattern, depicting a trantensional behaviour of the fault system along this sector.

Table 1
Seismogenic stress tensor.

Dataset	No	F (°)	σ_1		σ_2		σ_3		R
			Pl	Az	Pl	Az	Pl	Az	
A	165	6.6	0	320	89	203	1	50	0.6
B	37	6.5	52	355	35	145	15	246	0.3
C	68	6.2	8	140	73	258	15	48	0.6
D	60	4.9	1	320	88	196	2	50	0.6

N, F and R are, respectively, the number of events, the average misfit corresponding to the stress solution found and the measure of relative stress magnitude. Plunge and azimuth of the maximum (σ_1), intermediate (σ_2) and minimum (σ_3) compressive stress axes are reported. For the corresponding dataset, see the text.

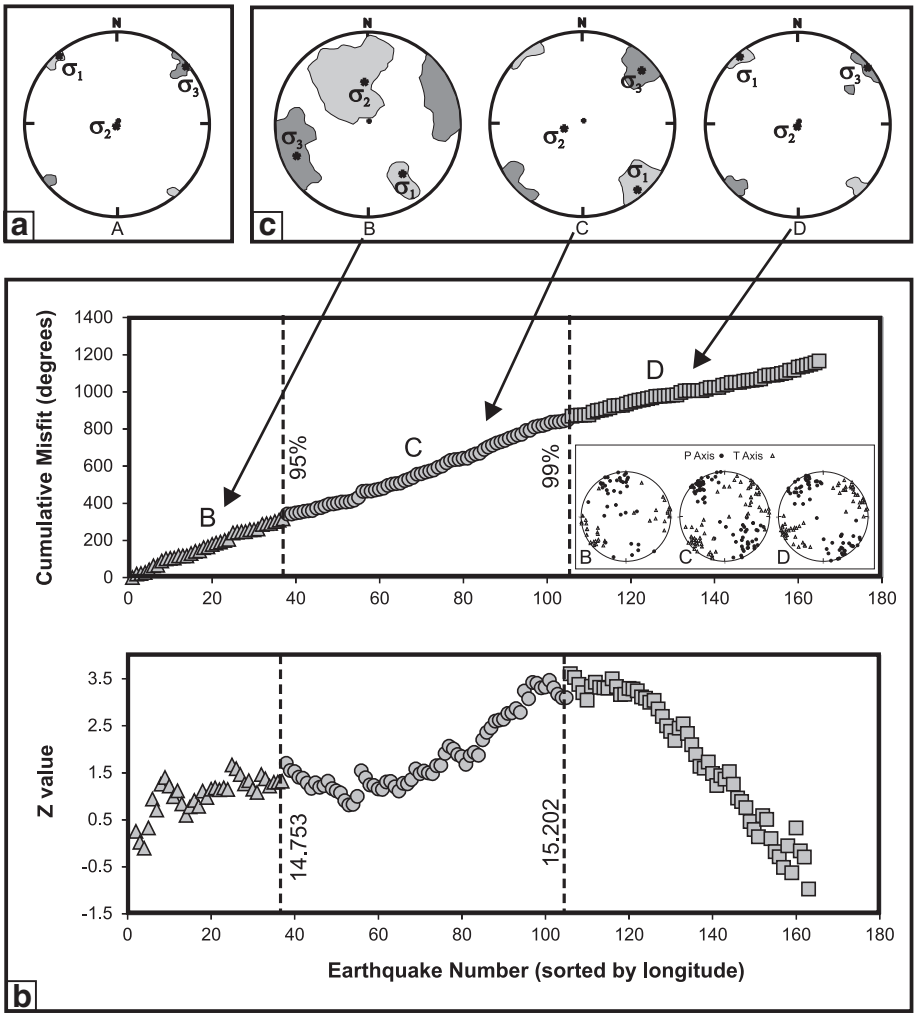

Fig. 7. (a) Orientations (lower-hemisphere projection) of the principal stress axes obtained by inverting the 165 FPSs. Grey areas indicate the 95% confidence limits of σ_1 and σ_3 orientations. (b) Cumulative misfit $\sum f(N)$ and Z-values versus earthquake number ordered for increasing longitude. Vertical dotted lines (labelled with the confidence levels and longitudes) indicate the change slopes of neighbouring segments. In the inset the projection of P and T directions for each group of data (B, C and D). See text for details. (c) Lower-hemisphere projection of the directions of the principal stress axes obtained for the three sub-sectors. Conventions as in (a).

In particular, on the eastern side of the fault system, IM02 and HMDC move in agreement with the NNW-directed motion of the plateau, while on the western side of the Scicli–Ragusa Fault System, HVZN moves toward NW. Using a mean N10°E fault trend and by applying a vector decomposition of the geodetic velocities of stations located across the northern sector of SRFS, we estimated a left-lateral strike–slip component of 1.2 mm/yr and a tensile component of 1.5 mm/yr, respectively. CONS station, although excluded from the vector decomposition because its motion is biased by large uncertainties, shows a motion which is compatible with the estimated components of motion. Conversely, based on velocities estimated at HSCI and HMDC sites, the southern sector of SRFS is characterised by a left-lateral strike–slip component of 0.5 mm/yr, while the component orthogonal to the fault trend is negligible.

The strain-rate field (Fig. 9b) clearly evidences as the Scordia–Lentini Graben (SLG) and the Catania Plain (CP) areas are dominated by a ~200 nanostrain/yr contractional belt with shortening axis oriented along the prevailing N–S direction. Along the coastal area, northward of the Augusta Basin, a local contractional belt, showing shortening axis oriented along the E–W direction, can be recognised. The southern-central sector of the plateau is characterised by a positive areal change of ~100 nanostrain/yr with lengthening axis oriented along the NW–SE direction, while in proximity of the Scicli–Ragusa Fault System these axes are aligned to the NE–SW direction. To the west of the Scicli–Ragusa Fault System, the northern sector of the plateau shows a gentle negative areal change (~30 nanostrain/yr), passing toward a gentle positive areal change (~20 nanostrain/yr) southward.

5. Discussion

The extensive seismic and geodetic dataset analysed in this study, allow us to infer some main features of the current tectonic setting of a large sector of southern Sicily, including the Hyblean Plateau and the front of the Maghrebian Chain, as well as the Ionian Sea offshore. Considering the main results here achieved, different crustal blocks, providing clear evidences about the crustal segmentation of the foreland, can be identified. In particular, the Hyblean Plateau is separate in two blocks (the western and the eastern) by the Scicli–Ragusa Fault System, while the Hyblean–Maltese Escarpment Fault System represents the boundary between the eastern block of the plateau and the Ionian basin. As discussed later, both fault systems are tectonic structures which accommodate the deformation between different segments of the foreland.

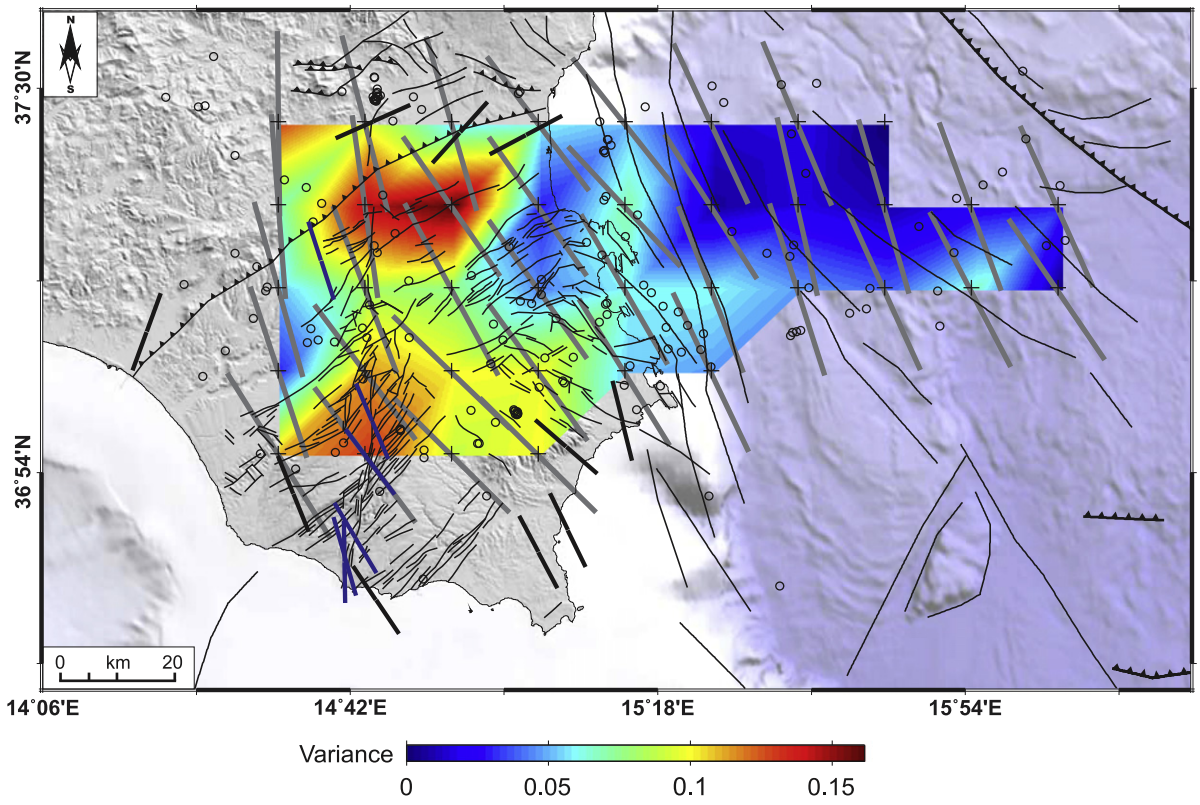

Fig. 8. Grey bars indicate the orientation of the σ_1 obtained by inverting the focal mechanisms inside the radius of 15 km around the grid cell, 15 × 15 km spaced (see text for details). Circles mark the hypocenters. The variance of the stress tensor at each node is colour-coded, with blue (low values) to red (high values) colours. Black bars indicate the orientation of the stress field coming from borehole breakout data (Ragg et al., 1999); blue bars indicate the orientation of the stress field coming from inversion of Quaternary fault slip data (Catalano et al., 2008).

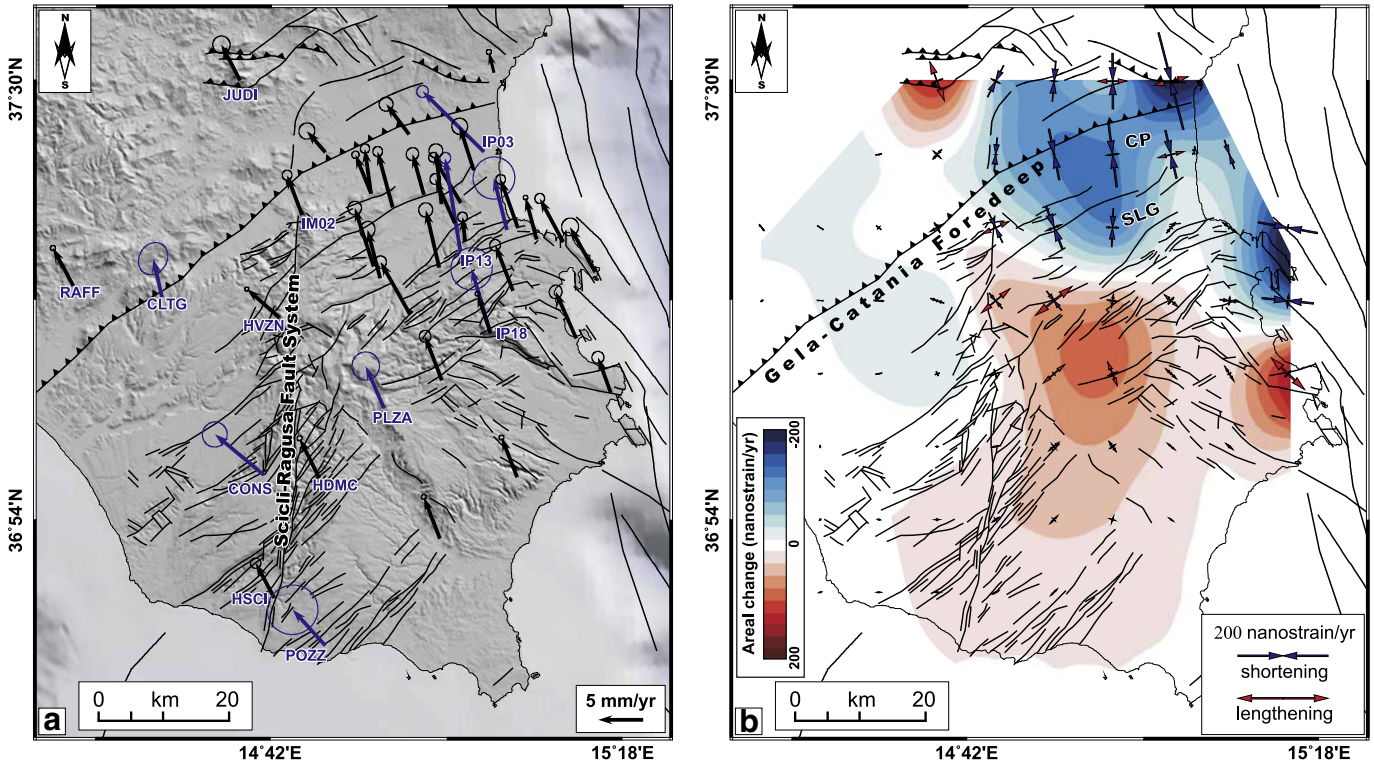

Fig. 9. (a) GPS velocities and 95% confidence ellipses in a fixed Eurasian reference frame. Solution for sites CONS and JUDI, analysed in Ferranti et al. (2008), were rigorously aligned to our solution by applying a seven-parameter Helmert transformation (obtained by finding the transformation that minimizes the RMS of differences between velocities of common sites). (b) Geodetic strain-rate parameters: the colour in background shows the rate of areal change, while the arrows represent the greatest extensional (red) and contractional (blue) horizontal strain-rates. CP, Catania Plain; SLG, Scordia–Lentini Graben.

The western sector is characterised by a low occurrence of seismic activity, which is mostly located along the SRFS and associated structures (Fig. 5). Fault plane solutions indicate that the crustal block is mainly subject to a strike–slip faulting regime with a maximum compressive stress axis with a nearly NNW–SSE attitude and a more relevant extensional component with respect to the other two blocks identified (Fig. 7). The NNW–SSE attitude is in agreement with the results coming from both i) boreholes breakout data acquired from wells (depth ranging from 2.3 km to 2.7 km) drilled during the 1980s (Ragg et al., 1999) and ii) structural analyses carried out along the SRFS (Catalano et al., 2008). Earthquake distribution, as well as the V_P anomalies, depict the geometry of the SRFS, while the focal mechanisms clearly indicate its kinematics, which is mainly left-lateral strike–slip. The geodetic data indicate an appreciable crustal deformation occurring along the SFRS: the northern sector of this fault system exhibits a left-lateral strike–slip component of ~1.2 mm/yr, coupled with a tensile component of ~1.5 mm/yr, while its southern sector is characterised by only a left-lateral strike–slip component of ~0.5 mm/yr. These slip-rate estimations refine previously estimations reported in Mattia et al. (2012) and are consistent with the geological rates reported in recent literature (~1.4 mm/yr since 0.85 Myr; see Catalano et al., 2008 for details). Whether and how the SFRS continues northward is unknown: few data are available to even speculate on this issue.

The eastern sector of the Hyblean Plateau is bounded by the SRFS to the left and by the Hyblean–Maltese Escarpment Fault System to the right. Distribution of seismic events (Fig. 5) points out that current brittle deformation of this area is mainly confined in its central sector (i.e. the area of the plateau including Siracusa, Noto, Palazzolo Acreide and Augusta), as also confirmed by the high V_P/V_S anomaly (Figs. 3 and 4) that can be interpreted in terms of increase of crack density, while is negligible in the others (i.e. northern and southern sectors). Focal mechanisms computed for this area are characterised by prevailing transtensive solutions, with a nodal plane oriented WNW–ESE to NW–SE (Fig. 6), fitting with the direction emphasized by the location of some event clusters (Fig. 5) and in agreement with outcropping geological features (e.g. Catalano et al., 2008; Grasso et al., 2000). Southward, the earthquakes are confined to the edge of the Plateau, where the tomography shows a discontinuity, down to 15 km of depth. From the morphological point of view, this area exhibits an escarpment (100–400 m), delimiting the Hyblean Plateau from the southern coastal plain, which several authors relate to a fault NE–SW oriented (i.e. the Avola Fault, see Bianca et al., 1999). The negligible or absent seismicity, southward of the Avola Fault–Pozzallo–Rosolini System line, coincides with the lack of mapped relevant faults. For this sector, a stable subhorizontal maximum compressive stress with a nearly NW–SE attitude was found.

Northward, along the Foredeep-Chain edge zone, the seismogenic layers and the V_P structure geometry indicate a progressive NW deepening of the Hyblean Plateau below the chain, down to 40 km (see Figs. 4 and 5). This finding is consistent with the northward-deepening seismicity, across central Sicily, suggested by Sgroi et al. (2012). In addition, GPS measurements available for this strip zone reveal a different deformation pattern between the two sectors of Hyblean Plateau across the SRFS. In detail, taking into account the relative motion between RAFF and HSCI continuous GPS sites, located northward and southward the foredeep, respectively (Fig. 9a), a lengthening of ~0.3 mm/yr can be estimated. This appears in disagreement with the active thrusting and transpression observed on the frontal belt of the foredeep by using seismotectonic data (Monaco et al., 1996). However, the lack of continuous GPS measurements covering the western sector does not allow any direct measurement of the occurrence of crustal deformation at a more local scale. Conversely, in the eastern sector, GPS data reveal that a contractional belt is the overriding feature of the Foredeep-Chain edge zone. In particular, a prevailing N–S oriented shortening of ~2.5 mm/yr is found along an area extending from the Scordia–Lentini Graben to the lower southern slope of Mt. Etna (Fig. 9a). There, several geological studies have shown that normal faults controlling the graben have been reactivated by reverse motion during the last 0.85 Myr (e.g. Bousquet and Lanzafame, 2004; Catalano et al., 2008). Despite the clear signals of active tectonics, very few seismic events have been registered in the last 20 years in the Scordia–Lentini Graben–Catania Plain area. This raises the question whether the lacking of seismic energy release, compared to the pronounced shallow deformation, could be correlated to a seismic gap, resulting in a very high seismic hazard for the area. However, in this area, a somewhat depth dependence of the stress field pattern has been observed. In particular, the maximum horizontal stress orientation found shows a prevailing NNW–SSE attitude, while at shallow depth, breakout wells data indicate an ENE–WSW direction (Fig. 8). The different stress orientation highlights that the deep stress pattern can be related to the ongoing convergence process (which represents the primary source of the stress field), while, at shallower depth it seems strongly influenced by secondary sources arising from local crustal structures related both i) to the downbending of the Hyblean crust beneath the Maghrebian Chain and ii) to the sub-surface geology (i.e. thick alluvial sediments filling the Scordia–Lentini Graben–Catania Plain area). According to previous studies (see Palano et al., 2012 and reference therein for an overview), we retain that part of the contraction arising from the main Eurasia–Nubia convergence is accommodated along this sector of the Foredeep-Chain edge zone. On the contrary, the western sector of the Hyblean Plateau moves in agreement with the central-western Sicily, transferring the Eurasia–Nubia convergence in the northern Sicily offshore (Palano et al., 2012).

The HMEFS, representing the faults-controlled tectonic boundary between the eastern sector of the Hyblean Plateau and the Ionian Sea, is characterised by the occurrence of considerable seismicity mainly located between the Gulf of Catania and Siracusa. Fault plane solutions indicate a prevailing strike–slip faulting with left-lateral slip along the ~N30°E direction and right-lateral motion along the conjugate ~N300°E one. This feature, coupled with the N–S to NNW–SSE striking of HMEFS and the sub-horizontal NW–SE striking σ_1-axis obtained for the offshore area, can lead to attribute a left-lateral shear component to this tectonic boundary. Accordingly, the right-lateral motion observed along the planes WNW–ESE oriented has to be considered as slip on secondary structures (i.e. Riedel shears).

Indeed, various hypotheses have been made in the last decade about the role and the kinematics of the HMEFS. In particular, based on the interpretations of seismic reflection profiles and bathymetric surveys, a prevailing extensional features (Argnani and Bonazzi, 2005), coupled with a dextral motion (see Doglioni et al., 2001; Catalano et al., 2008 and reference therein) was indicated. On the other hand, the left-lateral kinematic is supported by neotectonic observations (Adam et al., 2000) collected along the Quaternary faults located on the eastern border of the Hyblean Plateau. Adam et al. (2000) also suggest that the formation of oblique trending onshore grabens along the eastern margin of the Hyblean Plateau can be due to the coupled effects of two different stress fields: a left-lateral strike–slip stress regime, recognisable on the onshore side of HMEFS and an extensional one recognisable on the offshore side of HMEFS. The former stress field represents the regional field related to the plate convergence, while the latter represents a local field related to the topographic gradient across the HMEFS.

However, the left-lateral strike slip along roughly N–S trending faults is supported by the fault plane solution computed for the M = 5.4 December 13, 1990 earthquake (Amato et al., 1995) and by the focal mechanisms related to the earthquakes cluster occurring in the Catania Gulf (see Fig. 6).

Further to the east (Fig. 5), an event cluster, elongated in the NNW–SSE direction and located very close to the structure identified as the STEP fault by Polonia et al. (2011), can be identified. In addition, other earthquake alignments showing right-lateral strike–slip kinematics on NW–SE and WNW–ESE trending nodal planes (see Fig. 6), can be recognised in the Ionian Sea. By our data, we cannot solve the whole structural complexity characterising this Ionian sector, however, any

tectonic interpretation have to take into account that the structures drawn by our analysis segment this sector of the Ionian basin, releasing the dynamics of the Ionian lithosphere from the eastern Hyblean block.

6. Conclusive remarks

The main results presented and discussed in this study can be summarized as follows:

- The Scicli–Ragusa Fault System divides the Hyblean Plateau in two crustal blocks (the western and the eastern), while the Hyblean–Maltese Escarpment Fault System represents the boundary between the eastern sector of the plateau and the Ionian basin. Both fault systems are pre-existing tectonic structures which were reactivated to accommodate the deformation between different segments of the foreland.
- The western sector of the Hyblean Plateau moves in agreement with the central-western Sicily and is characterised by a low level of both ground deformation and seismic release.
- The northern portion of the eastern sector of Hyblean Plateau shows a prevailing N–S oriented shortening of ~2.5 mm/yr, accommodating the contraction arising from the main Eurasia–Nubia convergence.
- The Hyblean Plateau is subject to a general strike–slip faulting regime. At regional scale, the maximum horizontal stress shows a main mode trending NW–SE to NNW–SSE, in agreement with the Eurasia–Nubia direction of convergence. Locally, along the north-eastern sector of the Gela-Catania Foredeep a somewhat depth dependence of the stress field can be recognised.
- The left-lateral differential motion between the western and eastern Hyblean sectors and the Ionian one is accommodated along the SRFS, the HMEFS and their associated structures.

In conclusion, these findings provide useful elements to better understand the geodynamic scenario of central southern Mediterranean area and represent an improvement to the characterisation of the seismic sources that likely caused the large earthquakes in the past and could be the source regions for future events in southern Sicily and therefore to assess the earthquakes hazard of the region.

Supplementary data to this article can be found online at http://dx.doi.org/10.1016/j.tecto.2014.05.017.

Acknowledgements

We thank the Editor Laurent Jolivet and the reviewers Andrea Billi and Giusy Lavecchia for their critical reviews and constructive comments that greatly improved the paper. Haijiang Zhang is kindly acknowledged for providing the seismic tomography code (tomoDDPS). Helpful suggestions by Graziella Barberi are greatly appreciated, too. M.P. is grateful to S. Ferrara, who kindly provided some unpublished GNNS observations. Finally, we would like to thank all those people who contribute to the maintenance and development of the seismic and geodetic networks managed by INGV — Osservatorio Etneo and the analysts of "Gruppo Analisi Dati Sismici" for providing earthquake data.

References

Adam, J., Reuther, C.D., Grasso, M., Torelli, L., 2000. Active fault kinematics and crustal stresses along the Ionian margin of southeastern Sicily. Tectonophysics 326, 217–239.
Amato, A., Azzara, R., Basili, A., Chiarabba, C., Cocco, M., Di Bona, M., Selvaggi, G., 1995. Main shock and aftershocks of the December 13, 1990, Eastern Sicily earthquake. Ann. Geofis. 38, 255–266.
Argnani, A., Bonazzi, C., 2005. The Malta Escarpment fault zone offshore eastern Sicily: Pliocene-Quaternary tectonic evolution based on new multichannel seismic data. Tectonics 24, TC4009. http://dx.doi.org/10.1029/2004TC001656.
Azzaro, R., Barbano, M.S., 2000. Analysis of the seismicity of Southeastern Sicily: a proposed tectonic interpretation. Ann. Geofis. 43, 171–188.
Barreca, G., 2014. Geological and geophysical evidences for mud diapirism in southeastern Sicily (Italy) and geodynamic implications. J. Geodyn. http://dx.doi.org/10.1016/j.jog.2014.02.003.
Beutler, G., Moore, A.W., Mueller, I.I., 2008. The International Global Navigation Satellite Systems (GNSS) Service: developments and achievements. J. Geodesy 83 (3-4), 297–307. http://dx.doi.org/10.1007/s00190-008-0268-z.
Bianca, M., Monaco, C., Tortorici, L., Cernobori, L., 1999. Quaternary normal faulting in southeastern Sicily (Italy): a seismic source for the 1693 large earthquake. Geophys. J. Int. 139, 370–394.
Billi, A., Porreca, M., Faccenna, C., Mattei, M., 2006. Magnetic and structural constraints for the non-cylindrical evolution of a continental forebulge (Hyblea, Italy). Tectonics 25, TC3011. http://dx.doi.org/10.1029/2005TC001800.
Boccaletti, M., Cello, G., Tortorici, L., 1990. Strike–slip deformation as a fundamental process during the Neogene-Quaternary evolution of the Tunisian–Pelagian area. Ann. Tectonicae 4, 104–119.
Boschi, E., Guidoboni, E., Ferrari, G., Mariotti, D., Valensise, G., 2000. Catalogue of strong Italian earthquakes. Ann. Geofis. 43 (268 pp.).
Bousquet, J.C., Lanzafame, G., 2004. Compression and Quaternary tectonic inversion on the Northern edge of the Hyblean Mountains, foreland of the Appenine–Maghrebian chain in Eastern Sicily (Italy): geodynamic implications for Mt. Etna. GeoActa 3, 165–177.
Brancato, A., Hole, J.A., Gresta, S., Beale, J.N., 2009. Determination of seismogenic structures in southeastern Sicily (Italy) by high-precision relative relocation of microearthquakes. Bull. Seismol. Soc. Am. 99 (3), 1921–1936.
Butler, R.W.H., Grasso, M., La Manna, F., 1992. Origin and deformation of the Neogene-Recent Maghrebian foredeep at the Gela Nappe, SE Sicily. J. Geol. Soc. 149, 547–556.
Catalano, S., De Guidi, G., Romagnoli, G., Torrisi, S., Tortorici, G., Tortorici, L., 2008. The migration of plate boundaries in SE Sicily: influence on the large-scale kinematic model of the African promontory in southern Italy. Tectonophysics 449, 41–62. http://dx.doi.org/10.1016/j.tecto.2007.12.003.
Catalano, S., Romagnoli, G., Tortorici, G., 2010. Kinematics and dynamics of the Late Quaternary rift flank deformation in the Hyblean Plateau (SE Sicily). Tectonophysics 486, 1–14. http://dx.doi.org/10.1016/j.tecto.2010.01.013.
Chamot-Rooke, N., Rangin, C., Le Pichon, X., Working Group, D.O.T.M.E.D., 2005. DOTMED—deep offshore tectonics of the Mediterranean: a synthesis of deep marine data in eastern Mediterranean (CD-ROM). Mem. Soc. Geol. Fr. 177 (64 pp.).
Cocina, O., Neri, G., Privitera, E., Spampinato, S., 1997. Stress tensor computations in the Mount Etna area (southern Italy) and tectonic implications. J. Geodyn. 23 (2), 109–127.
DeMets, C., Gordon, R.G., Argus, D.F., 2010. Geologically current plate motions. Geophys. J. Int. 181, 1–80. http://dx.doi.org/10.1111/j.1365-246X.2009.04491.x.
Devoti, R., Esposito, A., Pietrantonio, G., Pisani, A.R., Riguzzi, F., 2011. Evidence of large scale deformation patterns from GPS data in the Italian subduction boundary. Earth Planet. Sci. Lett. 311, 230–241. http://dx.doi.org/10.1016/j.epsl.2011.09.034.
Doglioni, C., Innocenti, F., Mariotti, G., 2001. Why Mt Etna? Terra Nova 13 (1), 25–31. http://dx.doi.org/10.1046/j.1365-3121.2001.00301.x.
England, P., Molnar, P., 1997. Active deformation of Asia: from kinematics to dynamics. Science 278, 647–650. http://dx.doi.org/10.1126/science.278.5338.647.
Faccenna, C., Becker, T.W., Lucente, F.P., Jolivet, L., Rossetti, F., 2001. History of subduction and back-arc extension in the central Mediterranean. Geophys. J. Int. 145, 809–820. http://dx.doi.org/10.1046/j.0956-540X.2001.01435.x.
Ferranti, L., Oldow, J.S., D'Argenio, B., Catalano, R., Lewis, D., Marsella, E., Avellone, G., Maschio, L., Pappone, G., Pepe, F., Sulli, A., 2008. Active deformation in Southern Italy, Sicily and southern Sardinia from GPS velocities of the Peri-Tyrrhenian Geodetic Array (PTGA). Boll. Soc. Geol. Ital. 127 (2), 299–316.
Finetti, I.R., Del Ben, A., 1996. Crustal tectono-stratigraphic setting of the Pelagian Foreland from new CROP seismic data. In: Finetti, I.R. (Ed.), CROP Project: Deep Seismic Exploration of the Central Mediterranean and Italy, pp. 581–595 (Chapter 26).
Finetti, I.R., Lentini, F., Carbone, S., Del Ben, A., Di Stefano, A., Forlin, E., Guarnieri, P., Pipan, M., Prizzon, A., 2005. Geological outline of Sicily and lithospheric tectono-dynamics of its Tyrrhenian margin from CROP seismic data. In: Finetti, I.R. (Ed.), CROP: Deep Seismic Exploration of the Mediterranean Region, 15. Elsevier, pp. 319–376.
Gephart, J.W., 1990. Stress and the direction of slip on fault planes. Tectonics 9, 845–858.
Gephart, J.W., Forsyth, D.W., 1984. An improved method for determining the regional stress tensor using earthquake focal mechanism data: application to the San Fernando earthquake sequence. J. Geophys. Res. 89, 9305–9320.
Ghisetti, F., Vezzani, L., 1980. The structural features of the Iblean plateau and of the Monte Iudica area (South Eastern Sicily). A microtectonic contribution to the deformational history of the Calabrian Arc. Boll. Soc. Geol. Ital. 99, 57–102.
Gillard, D., Wyss, M., Okubo, P., 1996. Type of faulting and orientation of stress and strain as a function of space and time in Kilauea's south flank, Hawaii. J. Geophys. Res. 101, 16025–16042.
Grasso, M., Reuther, C.D., 1988. The western margin of Hyblean plateau: a neotectonic transform system on the SE Sicilian foreland. Ann. Tectonicae 2, 107–120.
Grasso, M., Pedley, H.M., Maniscalco, R., Ruggieri, R., 2000. Geological context and explanatory notes of the Carta Geologica del settore centromeridionale dell'Altopiano Ibleo. Mem. Soc. Geol. Ital. 55, 45–52.
Grasso, M., Behncke, B., Di Geronimo, I., Giuffrida, S., La Manna, F., Maniscalco, R., Pedley, H.M., Raffi, S., Schmincke, H.U., Strano, D., Sturiale, G., 2004. Carta geologica del bordo nord-occidentale dell'Avampaese Ibleo e del fronte della Falda di Gela. S.EL.C.A., Firenze.
Gruppo Analisi Dati Sismici, 2013. Catalogo dei terremoti della Sicilia Orientale - Calabria Meridionale (1999–2011). INGV-Catania (http://www.ct.ingv.it/ufs/analisti/catalogolist.php).
Guidoboni, E., Ferrari, G., Mariotti, D., Comastri, A., Tarabusi, G., Valensise, G., 2007. CFTI4Med, Catalogue of Strong Earthquakes in Italy (461 B.C.–1997) and Mediterranean Area (760 B.C.–1500). INGV-SGA (http://storing.ingv.it/cfti4med).

He, D.F., Yin, C., Du, S.K., Shi, X., Ma, H.S., 2004. Characteristics of structural segmentation of foreland thrust belts—a case study of the fault belts in the northwestern margin of Junggar Basin (in Chinese with English abstract). Earth Sci. Front. 11, 91–101.

Herring, T.A., King, R.W., McClusky, S.C., 2010. Introduction to GAMIT/GLOBK, Release 10.4. Massachusetts Institute of Technology, Cambridge MA pp. 1–48.

Husen, S., Kissling, E., Flueh, E., Asch, G., 1999. Accurate hypocentre determination in the seismogenic zone of the subducting Nazca plate in northern Chile using a combined on-/offshore network. Geophys. J. Int. 138, 687–701.

Iaffa, D.N., Sàbat, F., Muñoz, J.A., Carrera, N., 2013. Basin fragmentation controlled by tectonic inversion and basement uplift in Sierras Pampeanas and Santa Barbara System, northwest Argentina. Geol. Soc. Lond. Spec. Publ. 377, 101–117. http://dx.doi.org/10.1144/SP377.13.

Jordan, T.E., Schlunegger, F., Cardozo, N., 2001. Unsteady and spatially variable evolution of the Neogene Andean Bermejo foreland basin, Argentina. J. S. Am. Earth Sci. 14, 775–798. http://dx.doi.org/10.1016/S0895-9811(01)00072-4.

Lavecchia, G., Ferrarini, F., De Nardis, R., Visini, F., Barbano, M.S., 2007. Active thrusting as a possible seismogenic source in Sicily (southern Italy): some insights from integrated structural–kinematic and seismological data. Tectonophysics 445, 145–167. http://dx.doi.org/10.1016/j.tecto.2007.07.007.

Lu, H.F., Chen, C.M., Liu, Z.H., Jia, D., Wang, G.Q., Jia, C.Z., 2000. The structural features and origin of the Kuqa rejuvenation foreland thrust belt (in Chinese with English abstract). Acta Pet. Sin. 21, 18–24.

Malinverno, A., Ryan, W.B.F., 1986. Extension in the Tyrrhenian Sea and shortening in the Apennines as result of arc migration driven by sinking of the lithosphere. Tectonics 5 (2), 227–245. http://dx.doi.org/10.1029/TC005i002p00227.

Mantovani, E., Babbucci, D., Tamburelli, C., Viti, M., 2009. A review on the driving mechanism of the Tyrrhenian–Apennines system: implications for the present seismotectonic setting in the Central-Northern Apennines. Tectonophysics 476, 22–40. http://dx.doi.org/10.1016/j.tecto.2008.10.032.

Manuella, F.C., Brancato, A., Carbone, S., Gresta, S., 2013. A crustal-upper mantle model for southeastern Sicily (Italy) from the integration of petrologic and geophysical data. J. Geodyn. 66, 92–102.

Mattia, M., Bruno, V., Cannavò, F., Palano, M., 2012. Evidences of a contractional pattern along the northern rim of the Hyblean Plateau (Sicily, Italy) from GPS data. Geol. Acta 10, 1–9. http://dx.doi.org/10.1344/105000001705.

Michael, A.J., 1987. Use of focal mechanisms to determine stress: a control study. J. Geophys. Res. 92, 357–368.

Monaco, C., Tortorici, L., Nicolich, R., Cernobori, L., Costa, M., 1996. From collisional to rifted basins: an example from the southern Calabrian arc (Italy). Tectonophysics 266, 233–249. http://dx.doi.org/10.1016/S0040-1951(96)00192-8.

Musumeci, C., Di Grazia, G., Gresta, S., 2003. Minimum 1-D velocity model in Southeastern Sicily (Italy) from local earthquake data. J. Seismol. 7, 469–478.

Musumeci, C., Patanè, D., Scarfì, L., Gresta, S., 2005. Stress directions and shear-wave anisotropy: observations from local earthquakes in southeastern Sicily, Italy. Bull. Seismol. Soc. Am. 95 (4), 1359–1374. http://dx.doi.org/10.1785/0120040108.

Nicolich, R., Laigle, M., Hirn, A., Cernobori, L., Gallard, J., 2000. Crustal structure of the Ionian margin of Sicily: Etna volcano in the frame of regional evolution. Tectonophysics 329, 121–139. http://dx.doi.org/10.1016/S0040-1951(00)00192-X.

O'Connel, R.J., Budiansky, B., 1974. Seismic velocities in dry and saturated cracked solids. J. Geophys. Res. 79, 5412–5426.

Oldow, J.S., Ferranti, L., Lewis, D.S., Campbell, J.K., D'Argenio, B., Catalano, R., Pappone, G., Carmignani, L., Conti, P., Aiken, C.L.V., 2002. Active fragmentation of Adria, the north African promontory, central Mediterranean orogen. Geology 30 (9), 779–782. http://dx.doi.org/10.1130/0091-7613.

Palano, M., Cannavò, F., Ferranti, L., Mattia, M., Mazzella, M.E., 2011. Strain and stress fields in the Southern Apennines (Italy) constrained by geodetic, seismological and borehole data. Geophys. J. Int. 187, 1270–1282. http://dx.doi.org/10.1111/j.1365-246X.2011.05234.x.

Palano, M., Ferranti, L., Monaco, C., Mattia, M., Aloisi, M., Bruno, V., Cannavò, F., Siligato, G., 2012. GPS velocity and strain fields in Sicily and southern Calabria, Italy: updated geodetic constraints on tectonic block interaction in the central Mediterranean. J. Geophys. Res. 117. http://dx.doi.org/10.1029/2012JB009254 B07401.

Palano, M., Impresciа, P., Gresta, S., 2013. Current stress and strain-rate fields across the Dead Sea Fault System: constraints from seismological data and GPS observations. Earth Planet. Sci. Lett. 369–370, 305–316. http://dx.doi.org/10.1016/j.epsl.2013.03.043.

Parker, R.L., McNutt, M.K., 1980. Statistics for the one norm misfit measure. J. Geophys. Res. 85, 4429–4430.

Patacca, E., Sartori, R., Scandone, P., 1990. Tyrrhenian basin and Apenninic arcs. Kinematic relations since late Tortonian times. Mem. Soc. Geol. Ital. 45, 425–451.

Polonia, A., Torelli, L., Mussoni, P., Gasperini, L., Artoni, A., Klaeschen, D., 2011. The Calabrian Arc subduction complex in the Ionian Sea: regional architecture, active deformation, and seismic hazard. Tectonics 30, TC5018. http://dx.doi.org/10.1029/2010TC002821.

Presti, D., Billi, A., Orecchio, B., Totaro, C., Faccenna, C., Neri, G., 2013. Earthquake focal mechanisms, seismogenic stress, and seismotectonics of the Calabrian Arc, Italy. Tectonophysics 602, 153–175. http://dx.doi.org/10.1016/j.tecto.2013.01.030.

Ragg, S., Grasso, M., Müller, B., 1999. Patterns of tectonic stress in Sicily from borehole breakout observations and finite element modeling. Tectonics 18 (4), 669–685. http://dx.doi.org/10.1029/1999TC900010.

Reasenberg, P.A., Oppenheimer, D., 1985. Fortran computer programs for calculating and displaying earthquake fault-plane solutions. U.S. Geol. Surv., Open File Rept. 85-379 (109 pp.).

Scarfì, L., Giampiccolo, E., Musumeci, C., Patanè, D., Zhang, H., 2007. New insights on 3D crustal structure in Southeastern Sicily (Italy) and tectonic implications from an adaptive mesh seismic tomography. Phys. Earth Planet. Inter. 161, 74–85.

Scarfì, L., Langer, H., Scaltrito, A., 2009. Seismicity, seismotectonics and crustal velocity structure of the Messina Strait (Italy). Phys. Earth Planet. Inter. 177, 65–78. http://dx.doi.org/10.1016/j.pepi.2009.07.010.

Scarfì, L., Messina, A., Cassisi, C., 2013. Sicily and southern Calabria focal mechanism database: a valuable tool for local and regional stress-field determination. Ann. Geophys. 56 (1), D0109. http://dx.doi.org/10.4401/ag-6109.

Sgroi, T., de Nardis, R., Lavecchia, G., 2012. Crustal structure and seismotectonics of central Sicily (southern Italy): new constraints from instrumental seismicity. Geophys. J. Int. 189, 1237–1252.

Sirovich, L., Pettenati, F., 2001. Test of source parameters inversion of the intensities of a 54,000-death shock of the XVII Century in SE Sicily. Bull. Seismol. Soc. Am. 91 (4), 792–811.

Spampinato, C.R., Braitenberg, C., Monaco, C., Scicchitano, G., 2013. Analysis of vertical movements in eastern Sicily and southern Calabria (Italy) through geodetic leveling data. J. Geodyn. 66, 1–12. http://dx.doi.org/10.1016/j.jog.2012.12.002.

Tapponnier, P., Meyer, B., Avouac, J.P., Peltzer, G., Gaudemer, Y., Guo, S.M., Xiang, H.F., Yin, K. L., Chen, Z.T., Cai, S.H., Dai, H.G., 1990. Active thrusting and folding in the Qilian Shan, and decoupling between upper crust and mantle in northeastern Tibet. Earth Planet. Sci. Lett. 97 (3–4), 382–403. http://dx.doi.org/10.1016/0012-821X(90)90053-Z.

Thurber, C.H., Roecker, S., Ellsworth, W., Chen, Y., Lutter, W., Sessions, R., 1997. Two-dimensional seismic image of the San Andreas fault in the northern Gabilan Range, central California: evidence for fluids in the fault zone. Geophys. Res. Lett. 24, 1591–1594.

Torelli, L., Grasso, M., Mazzoldi, G., Peis, D., 1998. Plio-Quaternary tectonic evolution and structure of the Catania foredeep, the northern Hyblean Plateau and the Ionian shelf (SE Sicily). Tectonophysics 298 (30), 209–221.

Tortorici, L., Monaco, C., Mazzoli, S., Bianca, M., 2001. Timing and modes of deformation in the western Sicilian thrust system, Southern Italy. J. Pet. Geol. 24 (2), 191–211. http://dx.doi.org/10.1111/j.1747-5457.2001.tb00667.x.

Visini, F., de Nardis, R., Barbano, M.S., Lavecchia, G., 2009. Testing the seismogenic sources of the January 11th, 1693 Sicilian earthquake (Io X/XI): insights from macroseismic field simulations. Ital. J. Geosci. 128 (1), 147–156.

Visini, F., de Nardis, R., Lavecchia, G., 2010. Rates of active compressional deformation in central Italy and Sicily: evaluation of the seismic budget. Int. J. Earth Sci. 99, S243–S264. http://dx.doi.org/10.1007/s00531-009-0473-x.

Wessel, P., Bercovici, D., 1998. Interpolation with splines in tension: a Green's function approach. Math. Geol. 30, 77–93.

Wiemer, S., 2001. A software package to analyze seismicity: ZMAP. Seismol. Res. Lett. 72, 373–382.

Wyss, M., Lu, Z., 1995. Plate boundary segmentation by stress directions: southern San Andreas fault, California. Geophys. Res. Lett. 22, 547–550.

Wyss, M., Liang, B., Tanigawa, W.R., Xiaoping, W., 1992. Comparison of orientations of stress and strain tensor based on fault plane solutions in Kaoiki, Hawaii. J. Geophys. Res. 97, 4769–4790.

Zhang, H., Thurber, C., Bedrosian, P., 2009. Joint inversion for Vp, Vs, and Vp/Vs at SAFOD, Parkfield, California. Geochem. Geophys. Geosyst. 10, Q110032. http://dx.doi.org/10.1029/2009GC002709.

Zoback, M.L., 1992. First- and second-order patterns of stress in the lithosphere: the World Stress Map Project. J. Geophys. Res. 97 (B8), 11703–11728.